

# Development and implementation of a multi-scale model for matrix micro-cracking prediction in composite structures subjected to low velocity impact

Thomas Berton<sup>a,1</sup>, Farzin Najafi<sup>b,1</sup>, Chandra Veer Singh<sup>a,b,\*</sup>

<sup>a</sup> Dept. of Materials Science and Engineering, University of Toronto, 184 College St., Suite 140, Toronto, M5S 3E4, Canada

<sup>b</sup> Dept. of Mechanical and Industrial Engineering, University of Toronto, 5 King's College Road, Toronto, M5S 3G8, Canada

## ARTICLE INFO

### Keywords:

Damage mechanics  
Computational modelling  
Finite element analysis  
Impact behavior  
Micro-mechanics

## ABSTRACT

In this paper, a novel multi-scale damage model has been developed to predict the progression of matrix micro-cracking in a prototype car bumper under low-velocity impact. The methodology is based on FE micro-damage modelling to calibrate the parameters of a Synergistic Damage Mechanics model considering multi-axial loading, combined with a matrix micro-crack multiplication model. Python scripting was used to model a series of micro-mechanical FE models to determine the damage parameters, which were then used to simulate damage evolution at the structural scale, using a VUMAT subroutine. Following validation, the effects of the impactor's initial velocity, stacking sequence, rate-dependency and bumper's cross sectional profile have been evaluated for different material systems. The patterns of damage progression show that the damage model can accurately predict the progression of matrix micro-cracking, paving the way for the utilization of accurate multi-scale analysis tools in composite structures.

## 1. Introduction

Composite materials are being increasingly used in structural applications such as the aerospace, marine and construction sectors, due to their high mechanical performance and lower density as compared to traditional materials [1,2]. The automotive sector is becoming especially important for novel composites because of strict governmental regulations that are requiring automakers to reduce car weight and greenhouse gas emissions [3–5]. In service, automotive structures can be subjected to impact, for example from pedestrians, road infrastructure, hail, and road debris. Therefore, the impact performance needs to be optimized to ensure the reliability of automotive components. As such, novel composite material systems have been successfully manufactured with improved impact response [6–12], which shows that impact performance can be improved for composites by optimizing the structure. However, under low-velocity impact (LVI), the evolution of micro-damage mechanisms might be barely visible, while they might significantly degrade mechanical properties, which motivates the need for an accurate model to predict progressive damage. A damage model for impact damage should be able to relate the laminate material properties, including ply thickness, stacking sequence and material system to the evolution of damage throughout the structure. Such a model would allow engineers to improve the performance

of mechanical structures subjected to LVI.

Under LVI, a complex sequence of micro-damage mechanisms begins at the fiber-matrix interface through debonding and microcrack nucleation. These microcracks grow through the thickness of the ply and the width of the component, but they do not cause immediate failure. Microcracks are a pre-critical damage mode and do not cause failure of the composite. However, matrix microcracks eventually lead to critical damage modes, namely delamination and fiber fracture. If critical damage modes have occurred in the structure, their mechanical performance can decrease drastically, and their safe use cannot be guaranteed. In this paper, we use the convention proposed by Abrate [13] with low-velocity impact corresponding to speeds less than 100 m/s.

As loading increases, the microcrack density in each ply increases under the local ply tensile stress, leading to a degradation in stiffness. These damage mechanisms in laminates are characterized by their anisotropy, which arises from the stacking sequence of unidirectional plies with different properties along the fiber direction, and perpendicular to it. This anisotropy in progressive damage prevents the use of the damage models already used for traditional materials, such as metals. Nevertheless, the process of microcrack multiplication and ensuing performance degradation needs to be accounted for to properly understand the progressive failure process of a composite structure and

\* Corresponding author. Dept. of Materials Science and Engineering, University of Toronto, 184 College St., Suite 140, Toronto, M5S 3E4, Canada.

E-mail address: [chandraveer.singh@utoronto.ca](mailto:chandraveer.singh@utoronto.ca) (C.V. Singh).

<sup>1</sup> These authors contributed equally.

avoid critical damage which would lead to part failure.

To understand the damage response of advanced laminates under LVI, experimental approaches have been used in the past to investigate the effect of different parameters on micro-damage evolution [7–11,13–22]. Through a proper control of the material properties and geometrical configurations of the laminate, significant gains in impact performance have been achieved. For example, Sarasini et al. [8] found that damage evolution in flax/carbon fiber cross-ply depended on the presence of flax plies on the outside or middle section of the laminate. Ravandi et al. [9] studied the effect of inter-ply stitching on microcrack propagation. However, while such studies have been extremely useful in improving the understanding of impact damage, these experimental works are limited in their ability to generalize their findings to different material systems. Moreover, these studies are expensive, time-consuming and difficult to conduct. The results are also sensitive to environmental conditions such as humidity and temperature [23,24].

On the other hand, numerical studies of damage evolution under impact loading have also been conducted based on Continuum Damage Mechanics (CDM) [25–36]. In the majority of these papers, damage is typically implemented for each ply by using damage initiation criteria such as Hashin's [37–40], Puck's [28,41–43], Tsai-Wu [44–47] and LaRC [16,30,48,49], and CDM-based progression models. Delamination can be explicitly modelled by using Cohesive Zone Models (CZM) between each ply. Due to the explicit modelling of CZM, delamination prediction is usually limited to simple structures such as rectangular and curved geometries. Some of these models have been applied to car bumpers [50,51], allowing for improvements in structural design. In all cases, some parameters need to be determined through extensive experimental testing for each new laminate structure, which severely limits the range of applicability of these previous models.

To address these limiting issues in damage modelling in composite structures, a new model called Synergistic Damage Mechanics (SDM) has been developed which can help by-pass the need for complicated and costly experiments [52–55]. SDM is based on micromechanical Finite Element (FE) calculations, which calibrate the parameters of a CDM model, by-passing costly and complicated experiments. A stiffness degradation matrix is defined for symmetric laminates, and the evolution of Crack Opening Displacement (COD) with respect to crack density is calculated using a Representative Volume Element (RVE) of the laminate with cracks introduced in the plies. From these FE calculations, the evolution of stiffness with respect to crack density can be calculated without the use of any experimental measurements. Based on this modelling approach, crack multiplication can also be calculated using the crack initiation strain in each ply which can be obtained experimentally. The latest developments of SDM have incorporated multi-axial tensile loading effects [56,57] by using periodic RVEs of a cracked

laminate, as well as fatigue behavior [58]. The advantages of this model include its minimal reliance on experimental data for predictions, accurate modelling of complex multi-axial loading scenarios, and its relative simplicity, which allows for its implementation in FE software. Two previous papers have implemented the SDM model into commercial FE software to conduct structural analyses which included the effects of progressive damage [58,59]. The evolution of damage under fatigue loading in composite wind turbine blades was calculated.

In this paper, the SDM model has been implemented into commercial FE package in order to predict the pre-failure progressive matrix micro-cracking in a composite car bumper prototype under LVI loading. The focus of this paper is on understanding the evolution of pre-critical micro-cracking, before the onset of critical failure modes such as delamination. To our best knowledge, this is the first study to incorporate an accurate constitutive damage model for matrix micro-cracking in laminates for LVI of a complex structure under multi-axial loading that can also account for rate-dependent damage evolution. A subroutine has been developed, which can accurately calculate micro-crack multiplication in each ply of the laminate structure, as well as the in-plane stiffness matrix of the laminate. By incorporating rate-dependent damage evolution, the model is capable of predicting the performance of a realistic automotive structure and provides a fast and accurate tool for relating impact response to stacking sequences, ply thickness, and ply elastic properties. The study focuses on pre-failure damage evolution prior to the onset of critical failure modes such as delamination, which will be investigated in future work. However, delamination onset initiated from matrix micro-cracks is accounted for. The results of the study demonstrate the potential of the model to be used for the future robust design of composite structures.

## 2. Multi-scale progressive damage model

In order to predict the evolution of matrix micro-cracking in the structural laminates considered in this paper, a multi-scale modelling approach based on SDM is used. In this approach, an FE-based micro-damage model is created using commercial FE software to calculate the effect of matrix micro-cracks on the stiffness degradation of a laminate. The behavior of each layer of the laminate is assumed transversely isotropic. Micro-cracks are introduced in the plies of the model by disconnecting nodes across the thickness and width of the plies at the location of the crack faces. Cracks are assumed to be parallel to the fibers and to extend throughout the width and thickness of the ply, and to be uniformly spaced. An example RVE is shown in Fig. 1, showing the main assumptions and features of the model: the crack spacing is constant throughout the plies, the cracks are parallel to the fibers, and the local ply stress is used to predict matrix micro-cracking. Once cracks

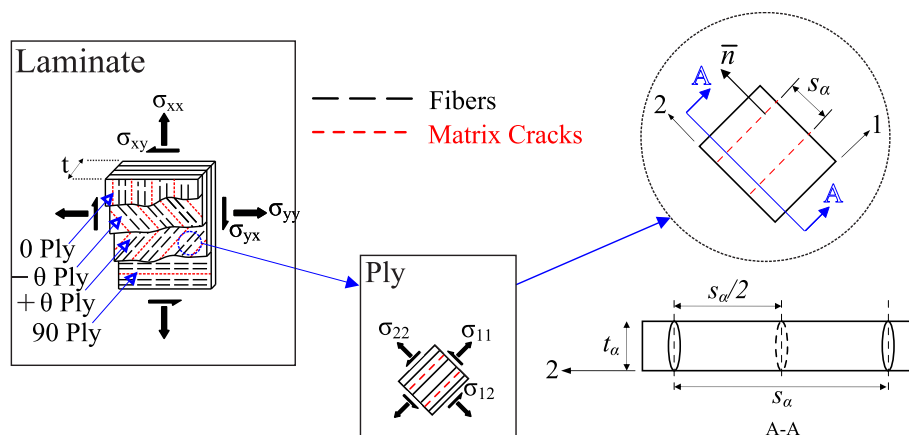


Fig. 1. Synergistic Damage Mechanics (SDM) RVE, showing the main features of the model, including uniform ply crack spacing, cracks parallel to the fibers in each layer, cracking in multiple off-axis orientations and multi-axial loading scenarios.

have been introduced, the reduced stiffness of the laminate is calculated. The constraining effects of adjacent plies is accurately captured through the Crack Opening Displacement (COD) which is used to calculate the stiffness of the laminate. Additionally, the effect of increasing crack density on stiffness evolution is captured by obtaining the relationship between COD and crack spacing. The crack spacing is varied by using Periodic Boundary Conditions (PBCs) in the RVE, and changing the dimensions of the RVE. The stiffness degradation model can be combined with an energy-based crack multiplication model to predict the evolution of micro-crack density under multi-axial loading. The crack multiplication model is also based on the evolution of COD with respect to crack density. This multi-scale approach can fully predict the constitutive behavior of any symmetric laminate undergoing complex multi-axial loading, with minimal experimental data for parameter calibration. In lieu of the complex experiments needed to obtain the relationship between applied load and performance degradation due to damage, this approach can be automated and easily repeated for a wide range of composite systems. The model is therefore significant step in understanding the evolution of pre-critical matrix microcracking leading to delamination.

### 2.1. Constitutive equations for cracked laminates

Each mode of damage ( $\alpha$ ) corresponds to a different ply crack orientation. Micro-cracking in the ply is represented by a damage matrix of the following form:

$$D_{ij}^{(\alpha)} = \frac{\kappa_\alpha t_\alpha^2}{s_\alpha t} n_i n_j = D_\alpha n_i n_j, \tag{1}$$

where  $t_\alpha$  is the thickness of the cracked ply with a given orientation,  $s_\alpha$  is the spacing between cracks in the ply,  $t$  is the total thickness of the laminate,  $n_i$  represents the components of the vector normal to the crack surface in the coordinate system of the laminate, and  $\kappa_\alpha$  accounts for the effect of adjacent plies as well as adjacent cracks on the COD of the ply crack. It is defined as the COD normalized by ply thickness and applied strain. The stiffness of a laminate that has undergone progressive ply cracking is given as:

$$C_{ij} = \begin{bmatrix} \frac{E_x^0}{1-\nu_{xy}^0\nu_{yx}^0} & \frac{\nu_{xy}^0 E_y^0}{1-\nu_{xy}^0\nu_{yx}^0} & 0 \\ \frac{\nu_{xy}^0 E_y^0}{1-\nu_{xy}^0\nu_{yx}^0} & \frac{E_y^0}{1-\nu_{xy}^0\nu_{yx}^0} & 0 \\ 0 & 0 & G_{xy}^0 \end{bmatrix} - \sum_{\alpha} b_\alpha D_\alpha \begin{bmatrix} 2a_1^{(\alpha)} & a_4^{(\alpha)} & 0 \\ a_4^{(\alpha)} & 2a_2^{(\alpha)} & 0 \\ 0 & 0 & 2a_3^{(\alpha)} \end{bmatrix}, \tag{2}$$

where  $C_{ij}$  is the  $3 \times 3$  stiffness matrix of a symmetric laminate written in Voigt notation, under plane stress conditions. In Eq. (2),  $E_x^0$ ,  $E_y^0$  are the Young's moduli in axial and transverse directions,  $\nu_{xy}^0$  and  $\nu_{yx}^0$  are the major and minor Poissons ratios respectively, and  $G_{xy}^0$  is the shear modulus of the undamaged laminate. The first term is the stiffness of the undamaged laminate with a specific stacking sequence and can be obtained from the ply properties. The second term represents the reduction in stiffness of the symmetric laminate due to matrix micro-cracks. It depends on the damage variable and a set of stiffness degradation parameters  $a_i^\alpha$ , where there are 4 parameters for each mode of damage  $\alpha$ . The parameter  $b_\alpha$  depends on the stacking sequence of the laminate, and is equal to 1 for the ply adjacent to the mid-plane of the laminate and 2 for all other plies.  $D_\alpha$  is a scalar which accounts for the crack spacing, the cracked ply thickness and the constraining effects of adjacent cracks and adjacent plies on the COD (see Eq. (1)). The effect of the cracked ply orientation on the stiffness degradation of the laminate is taken into account through the  $a_i^\alpha$  parameters, as well as  $\kappa_\alpha$ , which captures the evolution of COD with respect to crack density in the layer. The evolution of  $\kappa_\alpha$  with increasing crack density is obtained through the FE micro-damage model and is defined as:

$$\kappa_\alpha = \frac{(\overline{\Delta u_2})_\alpha}{\epsilon_{eff} t_\alpha} \tag{3}$$

where  $(\overline{\Delta u_2})_\alpha$  is the average COD calculated by

$$(\overline{\Delta u_2})_\alpha = \frac{1}{t_\alpha} \int_{-t_\alpha/2}^{t_\alpha/2} \Delta u_2^\alpha(z) dz \tag{4}$$

where  $t_\alpha$  is the thickness of the cracked ply, and  $\Delta u_2^\alpha(z)$  is the COD corresponding to mode of damage  $\alpha$  at coordinate  $z$  in the thickness direction of the ply. In Eq. (3),  $\kappa_\alpha$  is the normalized COD, and  $\epsilon_{eff}$  is the effective strain causing the cracks to open (i.e.  $\epsilon_{eff} = \epsilon_{22} + \nu_{12}\epsilon_{11} + \frac{1}{s} \nu_{21}\gamma_{12}$ ) which is used to incorporate the effects of multi-axial loading in the damage model [57]. The evolution of the COD in terms of the crack density in each layer is obtained from FE micro-damage modelling and is then fitted to an inverse sigmoidal function represented as follows:

$$\kappa_\alpha = \frac{c_1}{1 + (c_2 \rho_\alpha)^{c_3}} \tag{5}$$

where  $\rho_\alpha$  (or  $1/s_\alpha$ ) is the crack density corresponding to the mode of damage  $\alpha$ , and  $c_1$ ,  $c_2$  and  $c_3$  are the fitting parameters of the inverse sigmoidal function. By varying the crack density and calculating the COD and then the constraint parameter (Eq. (3)), a relationship between  $\rho_\alpha$  and  $\kappa_\alpha$  can be obtained, from which the fitting parameters are derived. Once the fitting parameters are obtained, the COD can be predicted for any micro-crack density using Eq. (5). Note that for a given crack density, multiple strain states are applied to the RVE. For each strain state,  $\epsilon_{eff}$  is obtained, as well as the COD. The COD is normalized by  $\epsilon_{eff}$ , and the evolution of the normalized COD with respect to crack density is defined. By using this effective strain, the effect multi-axial strain states on the COD can be accounted for, which is one of the major strengths of the model.

### 2.2. Energy model for damage evolution

The SDM model described in the previous section can predict the stiffness degradation for a given density of matrix micro-cracks. In order to predict the constitutive response of a laminate undergoing progressive damage, the evolution of the density of matrix micro-cracks with respect to the applied load is also required. An energy-based crack multiplication model has been used in this paper [56]. Based on the evolution of COD with respect to the density of matrix micro-cracks obtained using the FE micro-damage model (see Sec. 2.1), the energy density release rate for crack multiplication can be obtained using the following equation:

$$W_I = \frac{(\sigma_2^\alpha)^2 t_\alpha}{E_2} \left[ 2\tilde{u}_n^\alpha \left( \frac{s_\alpha}{2} \right) - \tilde{u}_n^\alpha(s_\alpha) \right] \tag{6}$$

Here,  $\tilde{u}_n^\alpha(s_\alpha)$  is the normalized COD for a crack spacing  $s_\alpha$  (equal to  $\kappa_\alpha$ ),  $E_2$  is the Young's modulus in the transverse direction of the ply, and  $\sigma_2^\alpha$  is the local ply transverse stress (perpendicular to the crack surfaces).  $\sigma_2^\alpha$  is calculated based on the local ply strain, and the linear elastic properties of the plies. Using the strain energy density release rate calculated with Eq. (6), a numerical procedure is used to predict crack density evolution versus applied global strain on the laminate. In order to predict crack multiplication, the critical energy density release rate  $G_{Ic}$  of the ply is required.  $G_{Ic}$  is itself calculated based on experimental data of crack multiplication versus applied strain. The energy-based crack multiplication model can also account for stochastic effects through a numerical procedure. In this procedure, each ply in the laminate is divided into a number of segments which can undergo matrix micro-cracking. At each increment of a for loop which runs through the ply segments, a stochastic value  $G_{Ico}$  is defined as follows:

$$G_{Ico} = G_o \left[ \log \left( \frac{1}{1-F} \right) \right]^{\frac{1}{m}} \tag{7}$$

where  $G_0$  and  $m$  are Weibull parameters, and  $F$  is randomly generated number between 0 and 1. The value of  $G_{Ic}$  obtained experimentally at the onset of crack multiplication is taken as the mean value of  $G_{Ic0}$  obtained through Eq. (7). The scatter in  $G_{Ic0}$  is taken as 10%. The value of  $G_{Ic0}$  is then used to calculate  $G_{Ic}$  based on the increase in resistance to crack multiplication with increasing crack density, which is modelled as follows:

$$G_{Ic} = G_{Ic0} + G_{Icr}(1 - \exp(-r\rho_c)) \quad (8)$$

where  $G_{Icr} = 0.8$  and  $r = 15$  are material parameters. Once the value of  $G_{Ic}$  taking into account stochastic effects and the increase in toughness with increasing crack density has been obtained, the criterion for crack multiplication is defined as:

$$\frac{W_I}{G_{Ic}} \geq 1 \quad (9)$$

If the criterion is satisfied, the number of cracks in the ply is incremented by 1, and the for loop continues to the next ply segment. As soon as the criterion is not satisfied anymore, the crack multiplication loop exits, at which point the total crack density in each ply can be calculated. The stiffness of the laminate is then updated based on Eq. (2), and the stress in the structure is obtained.

As shown by Nguyen and Gamby [60], the main effect of viscoelastic properties on crack multiplication in laminates is through the increase in  $G_{Ic}$  with increasing loading rate. This increase in critical energy release rate for crack multiplication is related to the rate-dependent failure properties of the epoxy matrix. Nguyen and Gamby developed a model which could account for crack multiplication in a CFRP cross-ply with increasing loading rate. In order to account for the viscoelastic properties of the composites in the present paper, a rate-dependent critical energy release rate for crack multiplication was defined based on this work [60]. The critical energy release rate for crack multiplication defined in Eq. (8) was modified according to the following relationships:

$$G_{Ic} = G_{Ic0} + G_{Icr}(1 - \exp(-r\rho_c)) \left( \frac{\dot{\sigma}}{\dot{\sigma}_r} \right)^{m_3} \quad (10)$$

where  $\dot{\sigma}_r = 1.3216$  MPa/min is a reference loading rate, and  $m_3 = 0.2$  describes the rate-dependence of  $G_{Ic}$ . Note that the loading rate refers to the local loading rate of the ply, which can be obtained from the local transverse strain rate and the linearly elastic properties of the plies. Moreover, the increase in critical energy also depends on the crack density. We should also remark that as per our previous works [61,62], viscoelasticity affects the behavior of laminates by affecting the rate-dependency of the critical energy release rate for crack multiplication, as per Eq. (10); the effect of viscoelastic properties on the material response of the laminate, in the absence of damage, can be ignored at the temperatures considered in this paper (room temperature).

The only experimental parameters needed in this multi-scale methodology are the elastic properties of the plies and the strains at which the first crack is initiated in each ply of the laminate. These values have been obtained from the literature for GFRP [63] and CFRP [64].

### 2.3. Prediction of delamination onset

The micro-mechanical RVE described previously is the fundamental component of SDM. Previous developments of the micro-mechanical model by Montesano and Singh [56,57] relied on the creation of complex geometries with cracks in multiple layers of multi-directional laminates, while enforcing periodic boundary conditions. These geometries did not account for delamination, as this was not the focus of the previous works. When the information obtained from the micro-mechanical FE models is used to calibrate the parameters of the SDM model, the structure of the laminate is homogenized at the structural

level. Some of the other models cited above [10,11,16,25] are based on explicit modelling of each layer of the laminate, which allowed the authors to use cohesive zone modelling to predict delamination. However, although these models have provided great insights into the evolution of damage in composite structures, SDM is capable of modelling interactions between matrix micro-cracking in different layers of the laminate under complex multi-axial loading scenarios.

To ensure the accuracy of the damage analysis, an energy-based approach has been implemented to predict the competition between matrix micro-cracking on the one hand, and delamination onset on the other. It has been assumed in the supplementary analysis that delamination initiates from the tips of the matrix micro-cracks. This framework is based on Nairn and Hu's seminal work on delamination induced by matrix micro-cracking [65]. The fundamental concept behind this model has been implemented in this work by calculating energy release rates for the onset of delamination at different crack densities. To do so, a cohesive zone model has been developed to predict delamination onset at different crack densities, thereby augmenting the complexity of the micro-mechanical model used in SDM. This energy release rate at a specific crack density and under a specific loading scenario has been compared to the energy release rate for crack multiplication, calculated using the energy-based crack multiplication model. More details of the overall modelling approach are given in section 4.2.

## 3. Numerical implementation

In this section, a hierarchical multi-scale framework is developed to implement the damage model in a numerical simulation package and used to evaluate the impact response of an automotive bumper subjected to a low velocity impact. Two separate codes are developed for this purpose. The process of micro-mechanical modelling is performed using an Abaqus-Python script which enables efficient calculation of the SDM model parameters. After the necessary parameters are captured from the micro-mechanical models, they are used to simulate the progressive damage of a bumper under impact in the form of matrix micro-cracking. A user-defined material subroutine (VUMAT) is developed to implement the constitutive equations during the impact simulation. The details of the implementation will now be discussed.

### 3.1. Micro-damage FE model

Fig. 2 shows the general steps of the numerical implementation of the multi-scale damage model. First, an Abaqus-Python script is developed to create and simulate the micro-mechanical RVEs. In order to accurately simulate a continuum body, two continuity conditions on the RVE faces, displacement and traction, must be satisfied. Therefore, before performing the simulations on the RVEs, one important step is to apply the periodic boundary conditions (PBCs) to the RVEs. Equation-type constraints are used to constrain each node pair on opposite faces of the RVEs. A complete description of applying PBCs in Abaqus is found in Ref. [66]. The next step is to calculate the undamaged material properties of a laminate with a specific stacking sequence using the micro-mechanical model. Three simulations are conducted for the undamaged RVE by applying strains in different directions: (i)  $\varepsilon_{xx}$ , (ii)  $\varepsilon_{yy}$ , and (iii)  $\gamma_{xy}$ . After conducting the simulations for an undamaged RVE, the undamaged material properties are obtained by calculating the average strains and stresses in the different directions. One may refer to Ref. [24] for more details of the procedure. The following step is to calculate the fitting parameters,  $c_1$ ,  $c_2$ , and  $c_3$ , in Eq. (5). A series of RVEs is generated with cracks in the different layers of the model, and with different side lengths, to simulate the effect of crack spacing (inverse of crack density). A strain state is applied to the RVE, and the corresponding values of  $(\overline{\Delta u_2})_\alpha$  and  $\kappa_\alpha$  (see Eq. (3) and Eq. (4)) are calculated for each damage mode. Multiple strain states are applied for a given crack density, so that the COD can be defined both in terms of crack density, and effective strain  $\varepsilon_{eff}$ . Next, the parameters  $c_1$ ,  $c_2$ , and  $c_3$  are

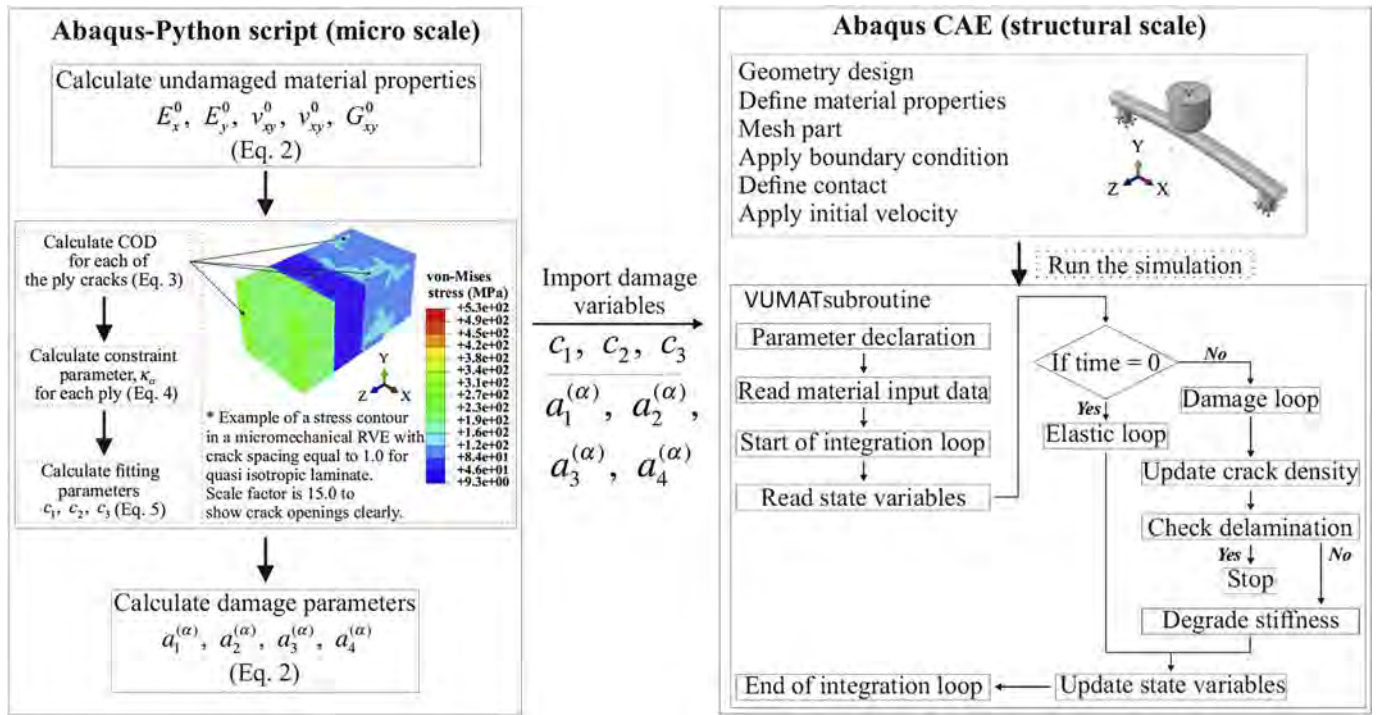


Fig. 2. General framework for the numerical implementation of the hierarchical multi-scale methodology.

obtained by fitting the evolution of  $\kappa_\alpha$  with respect to crack density (see Eq. (5)). Finally, the damage parameters  $a_{[1-4]}^{(\alpha)}$  are determined. For these parameters, an RVE is created by considering micro-cracking in only one ply at a time with a fixed crack density. Three strain states in different directions are applied to the RVE, as in the case of the undamaged RVE, and the average strains and stresses are evaluated. From these results, the stiffness of the laminate  $C_{ij}$  can be calculated for the fixed crack density. The COD corresponding to this certain crack density is obtained from the micro-mechanical model as well (see Eq. (5)), and the damage parameters  $a_{[1-4]}^{(\alpha)}$ , are calculated using Eq. (2). This process is repeated for each damage mode to calculate the corresponding damage parameters. A full description of the above mentioned procedure is provided in Ref. [57].

3.2. Impact test

Fig. 3 shows an automotive bumper subjected to a low-velocity external impactor. The impact event is simulated via the Abaqus/Explicit numerical package. The impactor is modelled as a rigid hemispherical shell with diameter 198 mm and mass 10.4 kg and is meshed with a 4-node 3-D bilinear quadrilateral (R3D4) element. As the impactor is rigid, a reference point is considered to represent the geometry of the impactor. The reference point is constrained in 5 degrees of freedom (X and Z translations and 3 rotations) and it is only free in the impact direction (Y translation). An initial velocity is applied to the reference point to perform the impact simulation. Two materials, IM7/5260 Carbon Fiber/Bismaleimide as carbon fiber reinforced polymer (CFRP) and VICOTEX NVE 913/28%/192/EC9756 glass/epoxy as glass fibre reinforced polymer (GFRP) are considered for this study and the materials properties are listed in Table 1.

The geometrical dimensions of the bumper are given in Fig. 3. It is meshed with a 4-node doubly curved shell element and reduced integration formulation (S4R). The transverse shear stiffness values were equal to 19.8 MN/m for GFRP and 23.24 MN/mm for CFRP. These values were obtained using CLT [1] and the stiffness properties of the plies and defined manually in Abaqus. The average element aspect ratio is about 2.0 to maintain an acceptable accuracy in the results (see Fig. 3

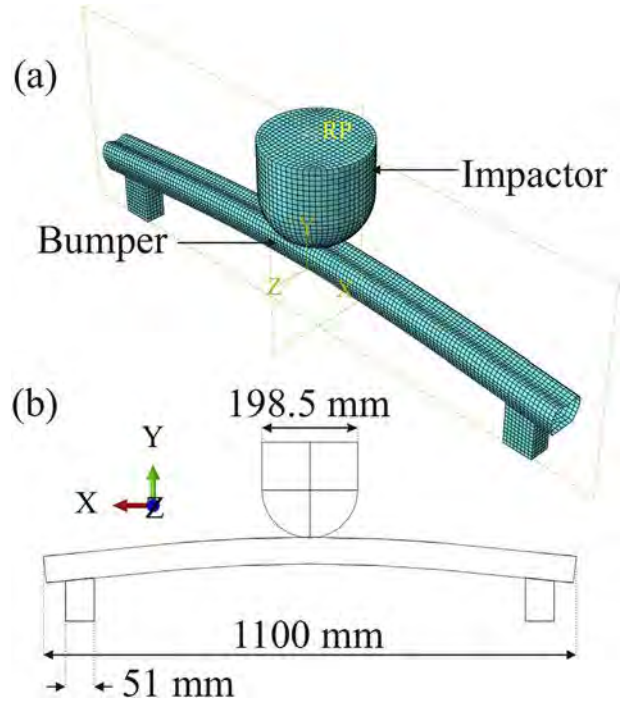


Fig. 3. Schematic of an automotive bumper subject to low velocity impact; (a) an example of the mesh pattern of the model, (b) geometrical dimensions of the model.

Table 1  
Material properties of CFRP and GFRP unidirectional lamina.

Material	Density	Orthotropic properties
CFRP	1550 kg/m <sup>3</sup>	$E_1 = 157 \text{ GPa}, E_2 = E_3 = 8.3 \text{ GPa}, \nu_{12} = \nu_{13} = 0.32, \nu_{23} = 0.32, G_{12} = G_{13} = 5.81 \text{ GPa}, G_{23} = 3.14 \text{ GPa}$
GFRP	1600 kg/m <sup>3</sup>	$E_1 = 45 \text{ GPa}, E_2 = E_3 = 14.6 \text{ GPa}, \nu_{12} = \nu_{13} = 0.32, \nu_{23} = 0.42, G_{12} = G_{13} = 4.95 \text{ GPa}, G_{23} = 5.14 \text{ GPa}$

for the mesh pattern). Moreover, as the subroutine is called at every integration point during the simulation procedure, the element size is considered larger than the micromechanical RVE in order to ensure the applicability of the constitutive equations [58]. The contact between the impactor and the bumper is defined via a general explicit contact algorithm in which the contact force is generated by utilizing the penalty enforcement contact method. The mass-scaling option is not considered for this analysis to prevent possible reduction in the accuracy of the results. Moreover, a tangential interaction with Coulomb friction coefficient is considered to account for the shear component of the surface traction  $\tau$ , which is related to the normal contact pressure by  $\tau = \mu p$ . The friction coefficient,  $\mu$ , depends on the surfaces of the contact materials and has been calculated for various materials; here  $\mu$  is considered to be 0.2 between the rigid surface and the composite laminate [25]. To implement the constitutive equations and incorporate the damage model, a vectored user-defined material (VUMAT) subroutine is developed. At each time increment and at every integration point in the elements, Abaqus calls the VUMAT subroutine to update the state of the material and the material mechanical response (i.e. stress and energy) based on the strain increment applied at the integration point. During this process, if the criterion of damage initiation is satisfied (see Eq. (9)), the updated crack density is obtained and the stiffness degradation is calculated to determine the stress increment at that integration point. This process continues until the end of the simulation. The flowchart of the VUMAT subroutine is presented in Fig. 2. Lastly, it should be noted that delamination onset is taken into account in the current model. Once delamination onset is predicted, the simulations are stopped. The focus is on matrix micro-cracking prior to delamination.

## 4. Results and discussion

### 4.1. Model verification

In order to verify the accuracy of the present damage model, a comparative study is undertaken here. The results of the present study are compared with those obtained by Schoeppner and Abrate [67]. They studied the impact response of laminate plates before and after delamination using experimental testing. In the test, a 12.7 mm × 12.7 mm laminate plate with stacking sequence  $[90/0]_{6s}$  was impacted by spherical nose impactor made of steel with diameter 25.4 mm, mass 3.1 kg and initial velocity 1.72 m/s (or initial kinematic energy equal to 4.61 J). The orthotropic properties of the laminate are given in Ref. [67]. Fig. 4 shows time histories of the contact force obtained in the present study alongside the results of Schoeppner and Abrate. Note that

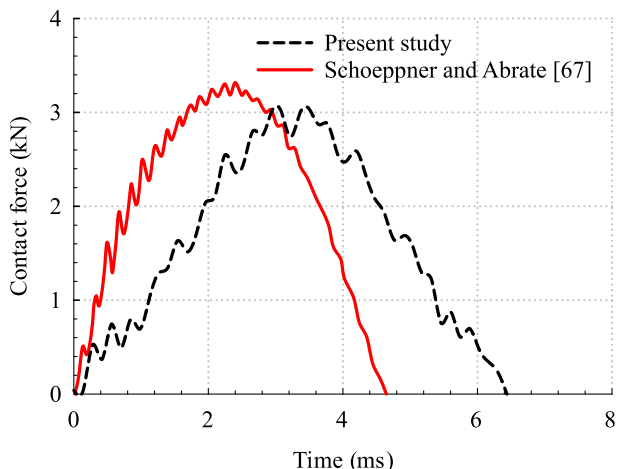


Fig. 4. Comparisons of time histories of contact force for a  $[90/0]_{6s}$  composite laminate between simulation and experiments.

for the experimental data shown in this figure, no significant damage (i.e. no delamination) was reported, allowing for a direct comparison with the damage model developed in this paper. The comparison of total contact time shows a relative discrepancy of about 25% between the results of the current study and those obtained by Schoeppner and Abrate. Three explanations can be provided for the differences between the results. First, the impact event takes place over small time intervals (milliseconds) and the results of Schoeppner and Abrate were obtained using experimental tests. Therefore, due to the complexity involved in measuring the displacement response experimentally, there might be small discrepancies between experimental results and computational results. Second, FE problems with contact definitions such as the impact simulations considered here can involve considerable numerical inaccuracies due to the complexity of the contact models. Moreover, when defining the interaction properties in a contact problem, different contact algorithms (i.e. general contact, surface to surface contact penalty and kinematic methods) can predict slightly different contact forces. Third, the impactor of present simulation is considered to be a rigid body, however, in the experimental test of [67], the impactor is made of steel which is a deformable material. Based on these remarks, the differences between simulation results and the experimental results shown in Fig. 4 are reasonable. It is worth mentioning that the same difference between experimental tests and numerical simulations for the time history of the contact force has also been reported by Ref. [43].

### 4.2. Prediction of delamination onset

The model used to predict delamination onset has been developed for a  $[0/90]_s$  cross-ply composite, as well as a quasi-isotropic  $[0/90/\mp 45]_s$  laminate, both with GFRP plies. The thickness of each layer is set to 1 mm for the cross-ply, and 0.5 mm for the quasi-isotropic laminate. Only the top-half of the symmetric laminate is modelled, while symmetric boundary conditions are applied to the mid-plane of the laminate. Each layer is assumed to be transversely isotropic, with elastic properties provided in Table 1. For the cross-ply, a micro-crack is introduced in the  $90^\circ$  ply by creating two separate parts which are connected to the top  $0^\circ$  ply using a cohesive zone model. For the quasi-isotropic laminate, an additional cohesive zone is used for the  $90^\circ/-45^\circ$  interface. The crack spacing has been varied by changing the length of the RVE. With varying crack spacing, the stress distribution at the micro-crack tip is affected, leading to a different driving force for delamination. The parameters of the surface-based CZM are provided in Table 2 of this document, and were obtained from Ref. [68].

A uniaxial strain is applied to the RVE in the axial direction (i.e. parallel to the  $0^\circ$  ply). The delaminated surface area is calculated at the post-processing stage. The strain energy released through delamination growth is also obtained, and divided by the delaminated surface area to obtain the strain energy release rate at a particular stress and crack density. This strain energy release rate for delamination is normalized as follows:

$$G_{norm}^{delam} = \frac{(\partial U / \partial a)}{\left( \frac{\sigma_x^2}{E_2} t_{ply} \right)} \tag{11}$$

where  $a$  is the delaminated area and  $U$  is the strain energy. In the case of the cross-ply, the delaminated area was straight across the width of the laminate. The normalized energy release rate has been plotted as a

Table 2  
Material properties of cohesive zone at the interface of the plies [68].

	Mode I	Mode II	Mode III
Normalized stiffness (GPa/mm)	1000	1000	1000
Strength (MPa)	35	65	65
Fracture energy (kJ/m <sup>2</sup> )	0.3	0.3	0.3

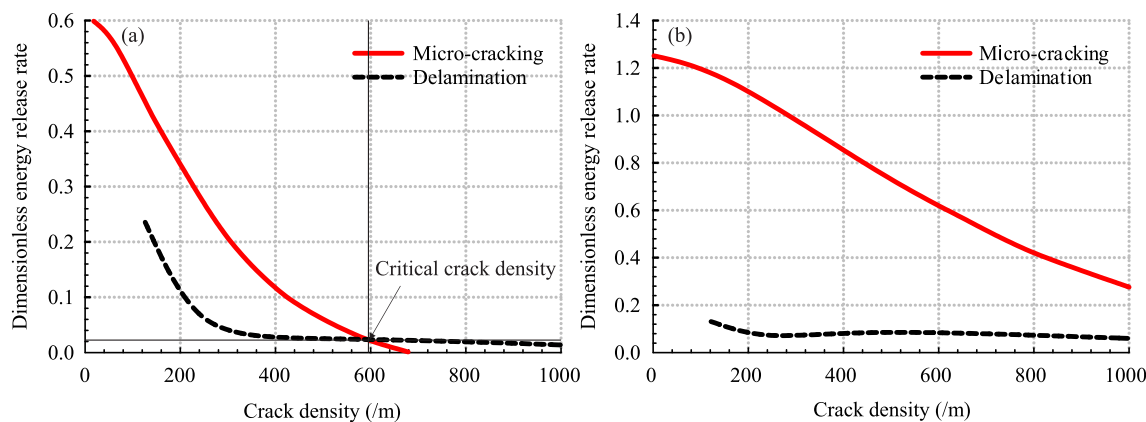


Fig. 5. Normalized energy release rates for delamination and matrix micro-cracking calculated using micro-damage modelling for the GFRP material system: (a) cross-ply, (b) quasi-isotropic laminate.

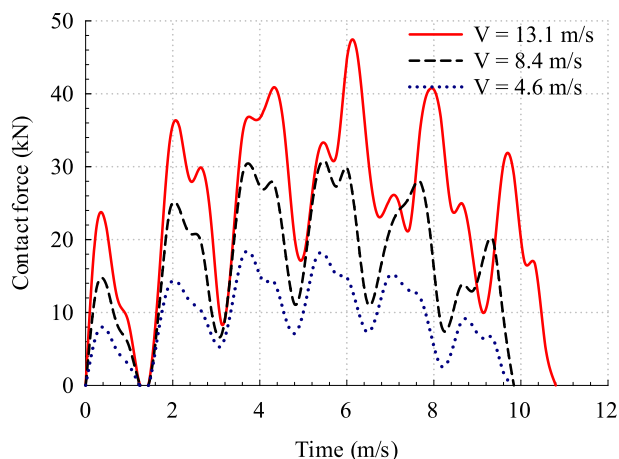


Fig. 6. Effect of the impactor's initial velocity on time histories of the contact force for a  $[0/90/\pm 45]_s$  GFRP laminate.

function of crack density for the  $90^\circ$  layer of the cross-ply in Fig. 5(a). Because of the change in stress field with different crack density, the normalized energy release rate for delamination onset changes with respect to crack density.

In order to determine whether matrix micro-cracking or delamination onset is more energetically favorable, the energy release rate for matrix micro-cracking in terms of crack density was also determined, using the energy-based micro-crack multiplication model described previously. The results of this analysis are plotted in Fig. 5(a) as well.

As can be observed from this figure, when energy release rates for delamination and micro-cracking are normalized, they depend on crack density. At approximately 0.6 cracks/mm, the normalized energy release rate for delamination becomes larger than the energy release rate for micro-crack multiplication. As per the analysis of Nairn and Hu [65], this shows that below this critical crack density, matrix micro-cracking will be more energetically favorable than delamination.

The same procedure was employed for the quasi-isotropic GFRP laminate with micro-cracks located in the  $90^\circ$  ply, with results shown in Fig. 5(b). Due to the lower thickness of the  $90^\circ$  ply, as compared to the cross-ply, it was found that micro-cracking was always more energetically favorable than delamination over the range of crack densities predicted by the energy-based damage model. Therefore, it is assumed that delamination initiating from micro-cracks is suppressed for this stacking sequence. However, in practice, delamination could be induced at the edges of the bumper, which cannot be modelled using the multi-scale framework, and is outside the scope of this work.

In order to determine whether delamination onset would occur in

the simulations conducted on the bumper for the cross-ply GFRP composite, a criterion for delamination has been implemented in the sub-routine using Eq. (11). If this energy release rate is larger than the critical energy release rate for delamination, obtained from the literature [68], and the crack density is larger than the critical value, delamination is assumed to have initiated, and the simulations are stopped as the model cannot predict the further growth in delaminated area.

Using this enhanced modelling approach, it was found that parts of the bumper would undergo delamination for the GFRP cross-ply material at an impactor velocity of 13.1 m/s. Below this velocity, delamination onset was not energetically favorable as compared to matrix micro-cracking. Therefore, results for this particular simulation case have not been included in this paper.

#### 4.3. Parametric study

In this section, a parametric study is performed on the effects of the impactor's initial velocity, laminate stacking sequence, bumper's cross section profile and rate-dependency. Fig. 3 shows the schematic of the assembled model of the rigid impactor and the composite bumper considered for this study. Note that the material properties and the geometric dimensions are given in Table 1 and Fig. 3 respectively. To analyze the effect of the impactor's initial velocity, three different sets of initial velocities, 4.6 m/s, 8.4 m/s, and 13.1 m/s are considered. Fig. 6 shows the time history of contact force for different initial velocities for the quasi-isotropic GFRP laminate. It can be seen that the velocity has a significant effect on the maximum contact force, however, the patterns in all results are almost identical. The contact force initially increases upon impact due to resistance from the bumper. It then decreases due to the dynamic response of the bumper. Following this first cycle, the contact force during the next cycle is greater, reaching 36 kN, instead of 24 at the first cycle when the initial velocity is set to 13.1 m/s. This larger force on the second cycle is due to the dynamic response of the bumper, which undergoes time-dependent deformation leading to a larger force on the impactor. The oscillations in all three curves are due to the dynamic behavior of the bumper.

Figs. 7–9 show the evolution of the crack density in each ply of the GFRP  $[0/90/\pm 45]_s$  laminate as a function of time. The crack densities plotted correspond to the maximum values reached throughout the bumper. The three different plots correspond to different initial impactor velocities. Looking first to Fig. 7, the crack multiplication process initiates first in the  $0^\circ$  ply, at approximately 0.2 ms after impact. This suggests that the local laminate stress is mainly transverse at this location. The crack density increases, until it saturates at 750 cr/m. At 1.6 ms after impact, damage initiates in the  $\pm 45^\circ$  plies. The crack density reaches a value 1200 cr/m in the  $-45^\circ$  while it only reaches 590 cr/m in the  $45^\circ$  because of its larger thickness. Crack multiplication

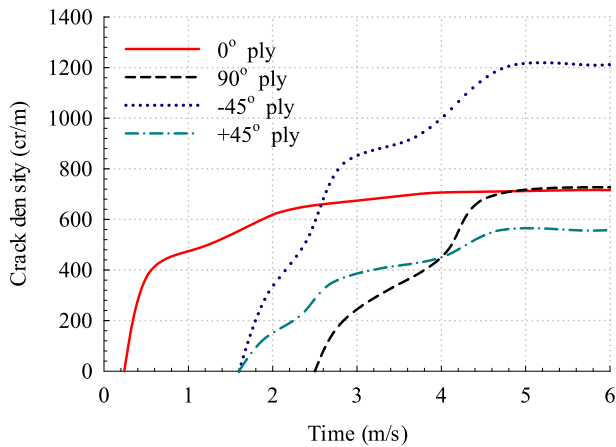


Fig. 7. Time history of evolution of crack density for different plies of a  $[0/90/\mp 45]_s$  GFRP laminate. Initial velocity of the impactor is equal to 4.6 m/s.

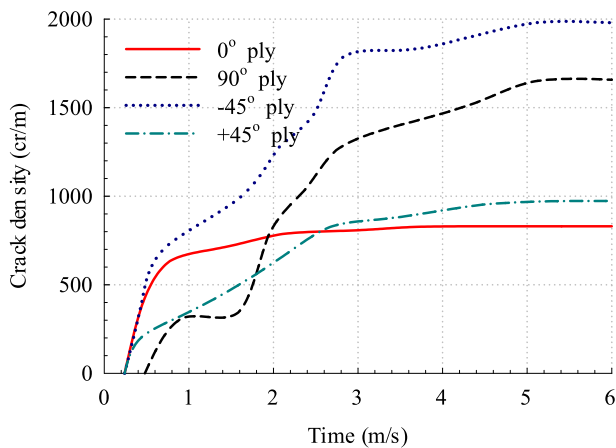


Fig. 8. Time history of evolution of crack density for different plies of a  $[0/90/\mp 45]_s$  GFRP laminate. Initial velocity of the impactor is equal to 8.4 m/s.

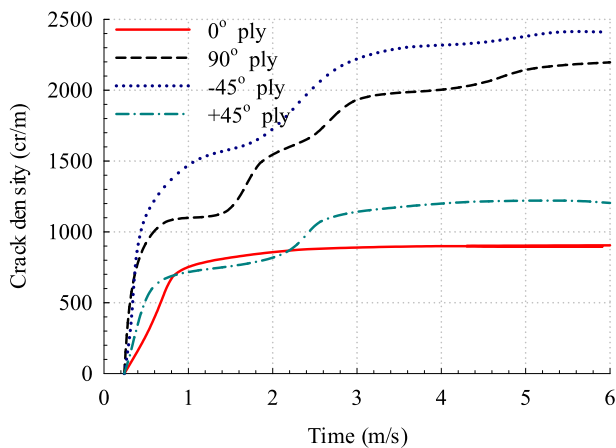


Fig. 9. Time history of evolution of crack density for different plies of a  $[0/90/\mp 45]_s$  GFRP laminate. Initial velocity of the impactor is equal to 13.1 m/s.

initiates in the  $90^\circ$  at 2.5 ms, reaching a maximum value of 750 cr/m. These trends for crack multiplication the different plies suggest a complex local loading scenario. We should note that the results of the simulations are written to the output files every 0.24 ms. Therefore, the results shown in Figs. 7–9 contain slight numerical inaccuracies due to the very small time scales at which crack multiplication evolves, which cannot be exactly captured with this relatively large time step.

When the impactor velocity is increased to 8.4 m/s, cracking initiates sooner in the  $\mp 45^\circ$ . This is due to the larger increase in local ply transverse stress with increasing velocity, which promotes crack multiplication. The maximum crack density in all plies increases relative to the simulation with lower impactor velocity. The same trends can also be observed when the impactor velocity is increased to 13.1 m/s. However, the crack density in the  $0^\circ$  ply does not increase significantly with higher impactor velocity. This saturation effect can be explained based on the crack multiplication model, in which the interaction between adjacent cracks prevents further increase in crack density.

The current model provides accurate insights into the evolution of sub-critical damage mechanisms which will eventually lead to failure of the structure. Understanding the progression of damage in the separate plies of the different laminates paves the way for failure models of laminates under dynamic impact loading. As has been shown in Figs. 7–9, the crack density in the  $0^\circ$  ply saturates, which can accurately be taken into account through the evolution of COD with respect to increasing crack density (see Eq. (5)). Moreover, the local ply stresses throughout the bumper induce a complex loading scenario on the different stacking sequences, which has caused complex patterns of damage evolution. To our knowledge, the SDM model, which uses fully periodic RVEs for calculating progressive damage evolution, is one of the only models which can account for these complex multi-axial loading scenarios with minimal experimental input. Taken together, we believe the observations reported in these figures demonstrate the effectiveness of the damage model.

Fig. 10 illustrates the contours of  $0^\circ$  ply crack density for the quasi-isotropic GFRP laminate for different initial velocities of the impactor. As seen in the three plots, the dominant damage occurs in the region of impact. As the impactor's velocity increases, additional damage is induced in the regions close to the boundaries. Under a velocity of 4.6 m/s, the maximum crack density in the  $0^\circ$  ply is 710 crack per meter (cr/m). It reaches 910 cr/m when the impactor velocity is increased to 13.1 m/s. This increase in crack density is due to the larger in-plane deformation that the impactor causes on the bumper as its velocity is increased, which drives crack multiplication.

Fig. 11 shows the results of displacement versus contact force and time histories of the contact force for a GFRP material system with three different laminate stacking sequences under an impactor velocity of 4.6 m/s. The  $[0/90/\mp 45]_s$  laminate has the highest maximum contact force compared to the others due to its higher stiffness. On the other hand,  $[0/90]_s$  laminate has the highest maximum displacement in the contact region, due to its much lower torsional stiffness relative to the other two laminates. Moreover, the shear stiffness of  $[0/90]_s$  is significantly degraded under impact due to damage, which explains the lower contact force. From Fig. 11(b), it can be seen that the  $[0/90/\mp 45]_s$  reaches a larger contact force (30 kN versus 23 kN for  $[0/90]_s$  and 28 kN for  $[-45/45]_s$ ). This is due to the larger stiffness properties of this stacking sequence relative to the other two laminates.

Fig. 12 shows the contact force - displacement curves and the contact force - time curves for three CFRP stacking sequences under an impactor velocity of 4.6 m/s. The trends observed for the CFRP material are the same here: the  $[0/90/\mp 45]_s$  laminate induces a larger contact force on the impactor, while the cross-ply is less resistant. However, the contact force caused by the CFRP composites is always higher than for GFRP (see Fig. 11). For example, the GFRP quasi-isotropic laminate induces a maximum contact force of 30 kN at 3.5 ms, while the CFRP quasi-isotropic laminate leads to a maximum force of 60 kN at 3.7 ms. This is due to the much larger in-plane stiffness of CFRP relative to GFRP.

Table 3 shows the maximum amount of damage in each laminate studied in this paper. The CFRP composites undergo less damage than the GFRP composites. This is due to the larger in-plane stiffness of CFRP, which constrains the COD and inhibits stiffness degradation. The  $[\mp 45]_s$  composite undergoes the most stiffness degradation due to its off-axis orientation. The cross-ply and the quasi-isotropic laminate undergo

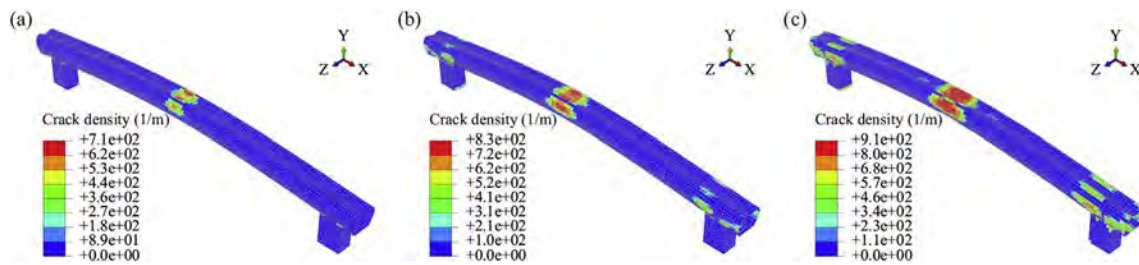


Fig. 10. Contour of 0° ply crack density for a  $[0/90/\pm 45]_s$  GFRP laminate for different impactor's initial velocity: (a)  $V = 4.6$  m/s, (b)  $V = 8.4$  m/s, and (c)  $V = 13.1$  m/s.

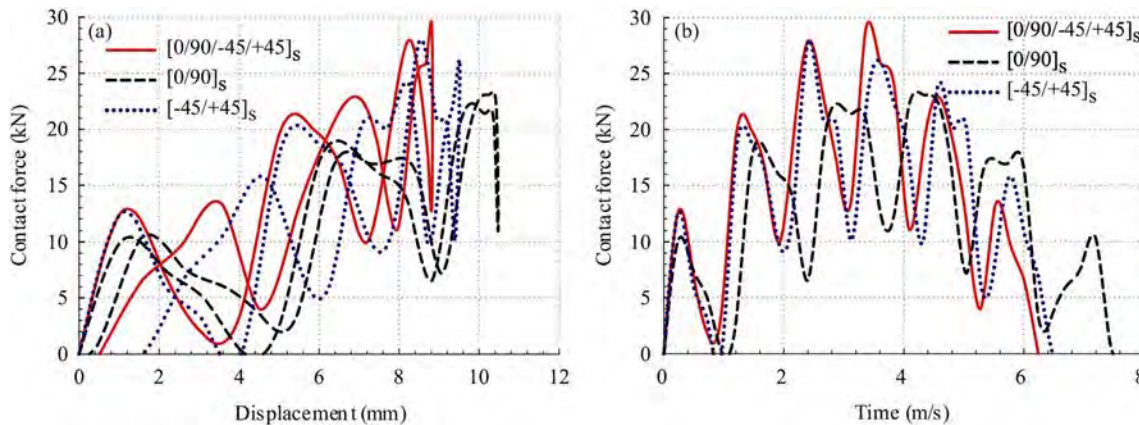


Fig. 11. Effect of laminate stacking sequence on (a) displacement versus contact force and, (b) time histories of contact force for GFRP laminates.

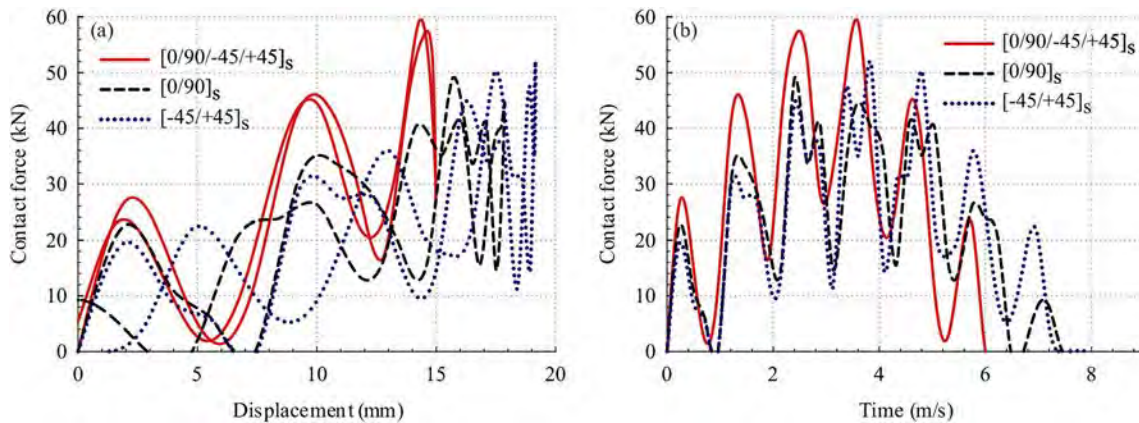


Fig. 12. Effect of laminate stacking sequence on (a) displacement versus contact force and, (b) time histories of contact force for CFRP laminates.

Table 3

Maximum degradation of material properties of laminates with different laminate stacking sequences due to impact event.

Laminate	$E_x$	$E_y$	$G_{xy}$	$\nu_{xy}^*$
CFRP, $[0/90/\pm 45]_s$	2.8%	4.6%	3.4%	+2.6%
CFRP, $[0/90]_s$	2.7%	3.7%	42.3%	-54.8%
CFRP, $[0/90/\mp 60]_s$	4.5%	2.0%	6.4%	-2.2%
CFRP, $[\mp 45]_s$	74%	74%	2.7%	+22%
GFRP, $[0/90/\pm 45]_s$	13.0%	17.6%	14.2%	+1.5%
GFRP, $[0/90]_s$	17.2%	18.2%	40.4%	-64.1%
GFRP, $[0/90/\mp 60]_s$	19.6%	10.6%	16.7%	-18.2%
GFRP, $[\mp 45]_s$	72.9%	72.9%	16%	+40%

\* Difference with pristine Poisson ratio.

similar amounts of stiffness degradation, however the shear modulus of the cross-ply is degraded more significantly due to the absence of  $\mp 45^\circ$  plies in its stacking sequence.

Fig. 13 shows the effect of rate - dependence for the  $[0/90/\mp 45]_s$  laminate. Rate-dependence has a slight effect on impact displacement and contact force evolution when the impactor has an initial velocity of 13.1 m/s. Including rate-dependence causes micro-cracking to be inhibited at higher loading rates. This leads to larger in-plane stiffness. This explains the slightly different contact force observed when rate-dependent cracking is accounted for. However, due to the low loading rates involved in low velocity impact, this effect is negligible, thus warranting the use of the simpler rate-independent crack multiplication model developed in this paper.

Fig. 14 shows the crack density contours for the  $[0/90/\mp 45]_s$  CFRP laminate with three different bumper cross-sections when the impactor velocity is 8.4 m/s. The first cross-section is square, and the maximum crack density in the  $0^\circ$  ply reaches 1000 cr/m. The second cross-section

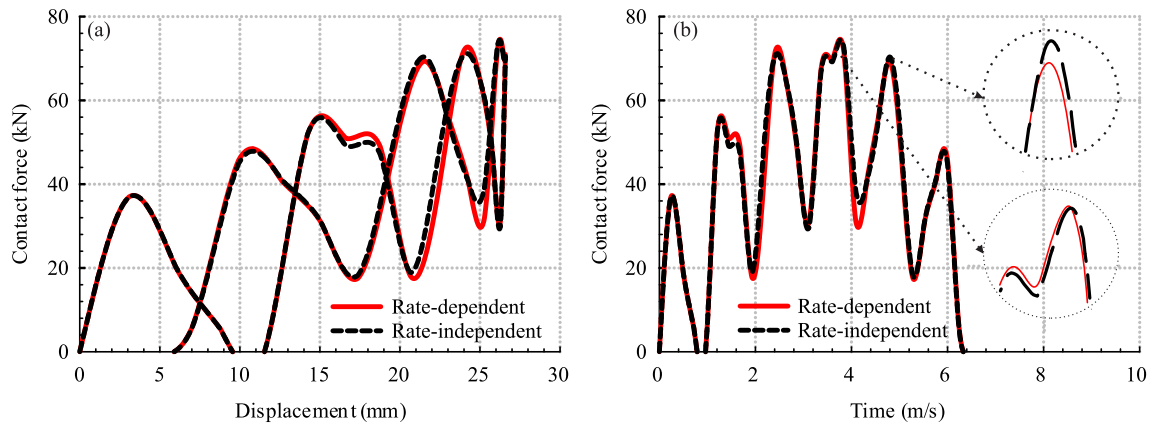


Fig. 13. Effect of rate-dependency on (a) displacement versus contact force and, (b) time histories of contact force for a GFRP  $[0/90/\pm 45]_s$  laminate.

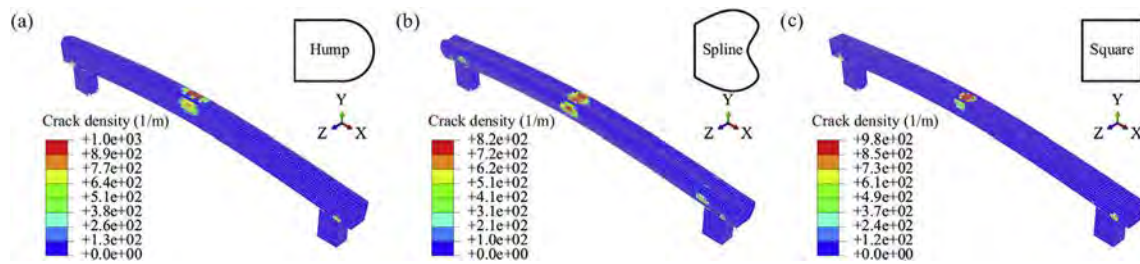


Fig. 14. Effect of the cross section profile of the bumper on stress and  $0^\circ$  crack density contours for a  $[0/90/\pm 60]_s$  CFRP laminate.

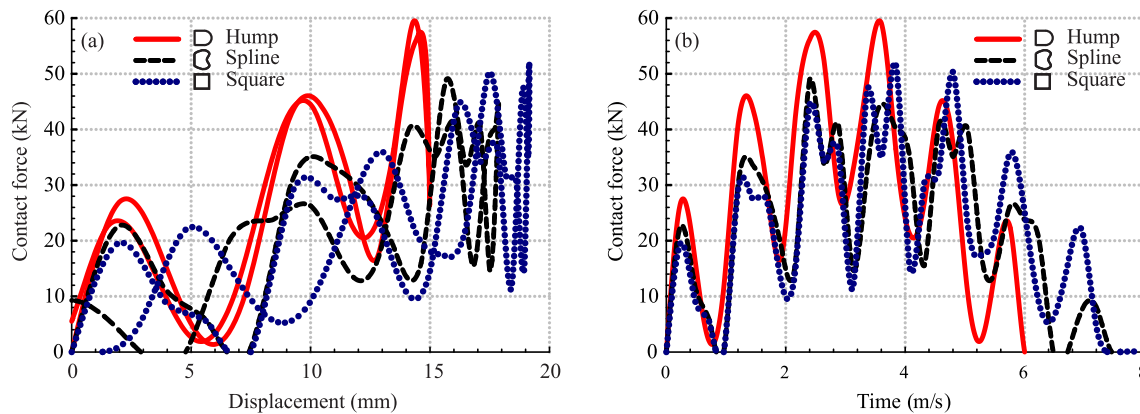


Fig. 15. Effect of bumper cross-section shapes on (a) displacement versus contact force and, (b) time histories of contact force for CFRP laminates for the  $[0/90/\pm 60]_s$  laminate.

**Table 4**  
Effect of the multi-axial loading formulation on maximum crack density of quasi isotropic GFRP laminate.

Ply orientation	Multi-axial	Uni-axial
$\mp 45^\circ$	1200 (cr/m)	1170 (cr/m)
$\mp 45^\circ$	2385 (cr/m)	2335 (cr/m)

is curved, and shows a maximum crack density of 820 cr/m, while the last cross-section contains grooves and the crack density reaches 980 cr/m. These differences between the different bumpers can be attributed to the shapes of the cross-section, which induce a different stress distribution upon impact, and therefore a different driving force for crack multiplication. The first bumper is more susceptible to damage evolution. These results therefore suggest that damage tolerance in composite car bumpers is related to the shape of the cross-section, which can be accounted for very accurately for using the methodology

presented in this paper.

Fig. 15 shows the effect of cross-section on the contact force and displacement of the bumper for the  $[0/90/\pm 60]_s$  CFRP laminate. There are some significant differences in the mechanical responses of the different bumpers: the bumper with a humped cross-sectional profile is much more rigid, leading to a maximum force of 60 kN on the impactor. The other two types of bumpers are more compliant. This can be attributed to the different distribution of damage in the bumper upon impact, as was illustrated in Fig. 14. It can also be attributed to the different stress distribution occurring in the different bumpers, which induces a different load-displacement response, even when neglecting the effects of damage. This suggests that cross-sectional shape partly governs the homogenized mechanical behavior of the bumper and that it has an effect on the damage evolution patterns throughout the structure.

Table 4 shows the results of maximum crack density using a simplified version of the crack multiplication model that does not account for multi-axial loading effects, and the model presented in section 2.2.

The laminate is a quasi-isotropic GFRP and the impactor's velocity is 13.1 m/s. The results are reported for  $\mp 45^\circ$  plies in which the multi-axial effects are dominant. Results show that adding the effect of multi-axial loading in the damage formulation leads to a higher prediction of the crack density as compared to the uni-axial formulation. This difference is due to the fact that the damage model takes into account out-of-plane Poisson contraction of the laminate, while the simplified uni-axial model does not. This three-dimensional effect is modelled accurately because of the way in which the micro-damage FE model is constructed: by using fully-periodic boundary conditions, the micro-damage model can predict multi-axial effects in an accurate way. The reader is referred to our previous works [57] for further details on the construction of such a model. This improvement allows for more accurate predictions of damage, which are required for applications where complex loading scenarios can occur.

## 5. Conclusion

In this paper, a damage model considering matrix micro-cracking in laminates has been used to predict the low-velocity impact response of a car bumper. FE micro-damage modelling is used to obtain the parameters of the damage model, in lieu of extensive and complicated experiments that have traditionally been used in CDM approach. The model is then implemented into Abaqus using a VUMAT subroutine. The LVI response for different stacking sequences and material systems under different impactor velocities is simulated using explicit dynamics in Abaqus. The main conclusions of this paper can be summarized as follows:

- GFRP laminates undergo more extensive deformation than the CFRP laminates, due to their lower in-plane stiffness, and more extensive damage evolution. The larger damage susceptibility of GFRP can be explained from the lower stiffness of the plies relative to CFRP, which limits the constraining effects of adjacent plies on the Crack Opening Displacements.
- It was found that for both CFRP and GFRP, the quasi-isotropic laminate underwent less deformation upon impact, and induced a larger contact force on the impactor; these observations were attributed to the larger bending stiffness of this stacking sequence.
- The effect of incorporating a rate-dependent crack multiplication model was also considered, and showed that rate-dependency only had minor effects of damage evolution, due to the low loading rates encountered in the simulations.
- Lastly, the effect of bumper cross-section shape was studied, and it was found that the damage evolution of composite car bumpers is sensitive to geometry; therefore, by optimizing the cross-sectional profile, the performance of the structure can be enhanced significantly against LVI.

It should again be noted that only pre-critical micro-cracking was considered in this study and critical damage modes such as delamination and fiber breakage will be left to future works. When delamination onset was predicted, the simulations were stopped.

In summary, the results of the parametric studies demonstrate the ability of the SDM modelling methodology to predict micro-cracking in the different plies of GFRP and CFRP laminates with different stacking sequences and cross-sectional shapes, as well as the mechanical response of damaged composites under dynamic loading.

## Acknowledgements

The authors would like to thank the Natural Sciences and Engineering Research Council (NSERC) of Canada, NSERC Automotive Partnership Canada (APC), Ford Motor Company of Canada and the University of Toronto for funding in support of this work.

## References

- [1] Herakovich C. *Mechanics of fibrous composites*. 1998.
- [2] Arif MF, Meraghni F, Chemisky Y, Despringre N, Robert G. In situ damage mechanisms investigation of PA66/GF30 composite: effect of relative humidity. *Compos B Eng* 2014;58:487–95. <https://doi.org/10.1016/j.compositesb.2013.11.001>
- [3] Kim HC, Wallington TJ. Life-cycle energy and greenhouse gas emission benefits of lightweighting in automobiles: review and harmonization. *Environ Sci Technol* 2013;47(12):6089–97. <https://doi.org/10.1021/es3042115>.
- [4] Kelly JC, Sullivan JL, Burnham A, Elgowainy A. Impacts of vehicle weight reduction via material substitution on life-cycle greenhouse gas emissions. *Environ Sci Technol* 2015;49(20):12535–42. <https://doi.org/10.1021/acs.est.5b03192>.
- [5] Greene D, Schafer A. Reducing greenhouse gas emissions from U.S. Transportation. *Tech Rep* 2013:1–66.
- [6] Taraghi I, Fereidoon A, Taheri-behrooz F. Low-velocity impact response of woven Kevlar/epoxy laminated composites reinforced with multi-walled carbon nanotubes at ambient and low temperatures. *J Mater* 2014;53:152–8. <https://doi.org/10.1016/j.matdes.2013.06.051>.
- [7] Bandaru AK, Chavan VV, Ahmad S, Alagirusamy R, Bhatnagar N. Low velocity impact response of 2D and 3D Kevlar/polypropylene composites. *Int J Impact Eng* 2016;93:136–43. <https://doi.org/10.1016/j.ijimpeng.2016.02.016>.
- [8] Sarasini F, Tirillò J, D'Altilia S, Valente T, Santulli C, Touchard F, et al. Damage tolerance of carbon/flax hybrid composites subjected to low velocity impact. *Compos B Eng* 2016;91:144–53. <https://doi.org/10.1016/j.compositesb.2016.01.050>.
- [9] Ravandi M, Teo W, Tran L, Yong M, Tay T. Low velocity impact performance of stitched flax/epoxy composite laminates. *Compos B Eng* 2017;117:89–100. <https://doi.org/10.1016/j.compositesb.2017.02.003>.
- [10] Yang B, Wang Z, Zhou L, Zhang J, Liang W. Experimental and numerical investigation of interply hybrid composites based on woven fabrics and PCBT resin subjected to low-velocity impact. *Compos Struct* 2015;132:464–76. <https://doi.org/10.1016/j.compstruct.2015.05.069>.
- [11] Simeoli G, Acierno D, Meola C, Sorrentino L, Iannace S, Russo P. The role of interface strength on the low velocity impact behaviour of PP/glass fibre laminates. *Compos B Eng* 2014;62:88–96. <https://doi.org/10.1016/j.compositesb.2014.02.018><http://linkinghub.elsevier.com/retrieve/pii/S135983681400095X>.
- [12] Yu GC, Wu LZ, Ma L, Xiong J. Low velocity impact of carbon fiber aluminum laminates. *Compos Struct* 2015;119:757–66. <https://doi.org/10.1016/j.compstruct.2014.09.054>.
- [13] Abrate S. *Impact on composite structures*. Cambridge: Cambridge University Press; 1998. <https://doi.org/10.1017/CBO9780511574504>.
- [14] Perillo G, Vedvik NP, Echtermeyer AT. Damage development in stitch bonded GFRP composite plates under low velocity impact: experimental and numerical results. *J Compos Mater* 2015;49(5):601–15. <https://doi.org/10.1177/0021998314521474>.
- [15] Petrucci R, Santulli C, Puglia D, Nisini E, Sarasini F, Tirillò J, et al. Impact and post-impact damage characterisation of hybrid composite laminates based on basalt fibres in combination with flax, hemp and glass fibres manufactured by vacuum infusion. *Compos B Eng* 2015;69:507–15. <https://doi.org/10.1016/j.compositesb.2014.10.031>.
- [16] Topac OT, Gozkluklu B, Gurses E, Coker D. Experimental and computational study of the damage process in CFRP composite beams under low-velocity impact. *Compos Part A Appl Sci Manuf* 2017;92:167–82. <https://doi.org/10.1016/j.compositesa.2016.06.023>.
- [17] Artero-Guerrero JA, Pernas-Sánchez J, López-Puente J, Varas D. Experimental study of the impactor mass effect on the low velocity impact of carbon/epoxy woven laminates. *Compos Struct* 2015;133:774–81. <https://doi.org/10.1016/j.compstruct.2015.08.027>
- [18] Scarponi C, Sarasini F, Tirillò J, Lampani L, Valente T, Gaudenzi P. Low-velocity impact behaviour of hemp fibre reinforced bio-based epoxy laminates. *Compos B Eng* 2016;91(2016):162–8. <https://doi.org/10.1016/j.compositesb.2016.01.048>.
- [19] Belingardi G, Vadori R. Low velocity impact tests of laminate glass-fiber-epoxy matrix composite material plates. *Int J Impact Eng* 2002;27(2):213–29. [https://doi.org/10.1016/S0734-743X\(01\)00040-9](https://doi.org/10.1016/S0734-743X(01)00040-9).
- [20] Choi HY, Downs RJ, Chang FK. A new approach toward understanding damage mechanisms and mechanics of laminated composites due to low-velocity impact. *J Compos Mater* 1991;25(1):992–1011.
- [21] Flores M, Mollenhauer D, Runatunga V, Bebernis T, Rapking D, Pankow M. High-speed 3D digital image correlation of low-velocity impacts on composite plates. *Compos B Eng* 2017;131:153–64. <https://doi.org/10.1016/j.compositesb.2017.07.078>
- [22] Bull DJ, Spearing SM, Sinclair I. Investigation of the response to low velocity impact and quasi-static indentation loading of particle-toughened carbon-fibre composite materials. *Compos Part A Appl Sci Manuf* 2015;74:38–46. <https://doi.org/10.1016/j.compositesa.2015.03.016>
- [23] Imielińska K, Guillaumat L. The effect of water immersion ageing on low-velocity impact behaviour of woven aramid-glass fibre/epoxy composites. *Compos Sci Technol* 2004;64(13–14):2271–8. <https://doi.org/10.1016/j.compscitech.2004.03.002>.
- [24] Gómez-del Río T, Zaera R, Barbero E, Navarro C. Damage in CFRPs due to low velocity impact at low temperature. *Compos B Eng* 2005;36(1):41–50. <https://doi.org/10.1016/j.compositesb.2004.04.003>.
- [25] Singh H, Namala KK, Mahajan P. A damage evolution study of E-glass/epoxy composite under low velocity impact. *Compos Part B* 2015;76:235–48. <https://doi.org/10.1016/j.compositesb.2015.05.069>.

- [org/10.1016/j.compositesb.2015.02.016](https://doi.org/10.1016/j.compositesb.2015.02.016).
- [26] Long S, Yao X, Zhang X. Delamination prediction in composite laminates under low-velocity impact. *Compos Struct* 2015;132:290–8. <https://doi.org/10.1016/j.compstruct.2015.05.037>.
- [27] Feng D, Aymerich F. Finite element modelling of damage induced by low-velocity impact on composite laminates. *Compos Struct* 2014;108(1):161–71. <https://doi.org/10.1016/j.compstruct.2013.09.004>.
- [28] Tan W, Falzon BG, Chiu LN, Price M. Predicting low velocity impact damage and Compression-After-Impact (CAI) behaviour of composite laminates. *Compos Part A Appl Sci Manuf* 2015;71:212–26. <https://doi.org/10.1016/j.compositesa.2015.01.025>.
- [29] Liao BB, Liu PF. Finite element analysis of dynamic progressive failure of plastic composite laminates under low velocity impact. *Compos Struct* 2017;159:567–78. <https://doi.org/10.1016/j.compstruct.2016.09.099>.
- [30] Lopes C, Sádaba S, González C, Llorca J, Camanho P. Physically-sound simulation of low-velocity impact on fiber reinforced laminates. *Int J Impact Eng* 2016;92:3–17. <https://doi.org/10.1016/j.ijimpeng.2015.05.014> <http://linkinghub.elsevier.com/retrieve/pii/S0734743X15001128>.
- [31] Zhang J, Zhang X. An efficient approach for predicting low-velocity impact force and damage in composite laminates. *Compos Struct* 2015;130:85–94. <https://doi.org/10.1016/j.compstruct.2015.04.023> <https://doi.org/10.1016/j.compstruct.2015.04.023>.
- [32] Xu Z, Yang F, Guan ZW, Cantwell WJ. An experimental and numerical study on scaling effects in the low velocity impact response of CFRP laminates. *Compos Struct* 2016;154:69–78. <https://doi.org/10.1016/j.compstruct.2016.07.029>.
- [33] Soto A, González EV, Maimí P, Martín de la Escalera F, Sainz de Aja JR, Alvarez E. Low velocity impact and compression after impact simulation of thin ply laminates. *Compos Part A Appl Sci Manuf* 2018;109(November 2017):413–27. <https://doi.org/10.1016/j.compositesa.2018.03.017> <https://doi.org/10.1016/j.compositesa.2018.03.017>.
- [34] de Moura MF, Gonçalves JP. Modelling the interaction between matrix cracking and delamination in carbon-epoxy laminates under low velocity impact. *Compos Sci Technol* 2004;64(7–8):1021–7. <https://doi.org/10.1016/j.compscitech.2003.08.008>.
- [35] Faggiani A, Falzon BG. Predicting low-velocity impact damage on a stiffened composite panel. *Compos Part A Appl Sci Manuf* 2010;41(6):737–49. <https://doi.org/10.1016/j.compositesa.2010.02.005> <https://doi.org/10.1016/j.compositesa.2010.02.005>.
- [36] Maio L, Monaco E, Ricci F, Lecce L. Simulation of low velocity impact on composite laminates with progressive failure analysis. *Compos Struct* 2013;103:75–85. <https://doi.org/10.1016/j.compstruct.2013.02.027> <https://doi.org/10.1016/j.compstruct.2013.02.027>.
- [37] Hashin Z. Failure criteria for unidirectional fiber composites. *J Appl Mech* 1980;47(2):329–34. <https://doi.org/10.1115/1.3153664>.
- [38] Tie Y, Hou Y, Li C, Zhou X, Sapanathan T, Rachik M. An insight into the low-velocity impact behavior of patch-repaired CFRP laminates using numerical and experimental approaches. *Compos Struct* 2018;190:179–88. <https://doi.org/10.1016/j.compstruct.2018.01.075> <https://www.sciencedirect.com/science/article/pii/S0263822317336851>.
- [39] Kim DH, Jung KH, Lee IG, Kim HJ, Kim HS. Three-dimensional progressive failure modeling of glass fiber reinforced thermoplastic composites for impact simulation. *Compos Struct* 2017;176:757–67. <https://doi.org/10.1016/j.compstruct.2017.06.031> <https://www.sciencedirect.com/science/article/pii/S0263822317309224>.
- [40] Gliszczynski A. Numerical and experimental investigations of the low velocity impact in GFRP plates. *Compos B Eng* 2018;138:181–93. <https://doi.org/10.1016/j.compositesb.2017.11.039> <https://www.sciencedirect.com/science/article/pii/S135983681633270X>.
- [41] Puck A, Schürmann H. Failure analysis of FRP laminates by means of physically based phenomenological models. *Fail. Criteria fibre-reinforced-polymer composites Elsevier*; 2004. p. 832–76. <https://doi.org/10.1016/B978-008044475-8/50028-7>. ISBN 9780080531571 <https://www.sciencedirect.com/science/article/pii/B9780080444758500287>.
- [42] Li N, Chen PH, Ye Q. A damage mechanics model for low-velocity impact damage analysis of composite laminates. *Aeronaut J* 2017;121(1238):515–32. <https://doi.org/10.1017/aer.2017.6> <https://www.cambridge.org/core/article/damage-mechanics-model-for-low-velocity-impact-damage-analysis-of-composite-laminates/238C9304BBA395FB4284EF9CE446ACD6>.
- [43] Shi Y, Swait T, Soutis C. Modelling damage evolution in composite laminates subjected to low velocity impact. *Compos Struct* 2012;94(9):2902–13. <https://doi.org/10.1016/j.compstruct.2012.03.039>.
- [44] Tsai SW. *Theory of composites design*. OH: Think composites Dayton; 1992. ISBN 0961809035.
- [45] Tay TE, Tan VB, Deng M. Element-failure concepts for dynamic fracture and delamination in low-velocity impact of composites. *Int J Solid Struct* 2003;40(3):555–71. [https://doi.org/10.1016/S0020-7683\(02\)00623-6](https://doi.org/10.1016/S0020-7683(02)00623-6) <https://www.sciencedirect.com/science/article/pii/S0020768302006236>.
- [46] Lin J, Guan Y, Li J, Huang L, Naceur H, Coutellier D. Meshless modelling of low-velocity impacting damage for composite laminates. *Ferroelectrics* 2018;527(1):93–106. doi:10.1080/00150193.2018.1450543 <https://doi.org/10.1080/00150193.2018.1450543>.
- [47] Shivakumar KN, Elber W, Illg W. Prediction of low-velocity impact damage in thin circular laminates. *AIAA J* 1985;23(3):442–9. <https://doi.org/10.2514/3.8933> <http://arc.aiaa.org/doi/10.2514/3.8933>.
- [48] Davila C, Jaunky N, Goswami S. Failure criteria for FRP laminates in plane stress. 44th AIAA/ASME/ASCE/AHS/ASC struct. Struct. Dyn. Mater. Conf. 2003. p. 1991.
- [49] Pinho ST, Dávila CG, Camanho PP, Iannucci L, Robinson P. Failure models and criteria for FRP under in-plane or three-dimensional stress states including shear non-linearity. *Tech. Rep.* 2005:1–69. doi:NASA/TM-2005-213530.
- [50] Marzbanrad J, Alijanpour M, Kiasat MS. Design and analysis of an automotive bumper beam in low-speed frontal crashes. *Thin-Walled Struct* 2009;47(8–9):902–11. <https://doi.org/10.1016/j.tws.2009.02.007>.
- [51] Hosseinzadeh R, Shokrieh MM, Lessard LB. Parametric study of automotive composite bumper beams subjected to low-velocity impacts. *Compos Struct* 2005;68(4):419–27. <https://doi.org/10.1016/j.compstruct.2004.04.008>.
- [52] Singh CV, Talreja R. Analysis of multiple off-axis ply cracks in composite laminates. *Int J Solid Struct* 2008;45(16):4574–89. <https://doi.org/10.1016/j.ijsolstr.2008.04.004>.
- [53] Singh CV. A higher order synergistic damage model for prediction of stiffness changes due to ply cracking in composite laminates. *Comput Mater Continua (CMC)* 2013;34(3):227–49.
- [54] Singh CV, Talreja R. A synergistic damage mechanics approach for composite laminates with matrix cracks in multiple orientations. *Mech Mater* 2009;41(8):954–68. <https://doi.org/10.1016/j.mechmat.2009.02.008>.
- [55] Singh CV, Talreja R. A synergistic damage mechanics approach to mechanical response of composite laminates with ply cracks. *J Compos Mater* 2012;47:2475–501. <https://doi.org/10.1177/0021998312466121>.
- [56] Montesano J, Singh C. Predicting evolution of ply cracks in composite laminates subjected to biaxial loading. *Compos B Eng* 2015;75:264–73. <https://doi.org/10.1016/j.compositesb.2015.01.039>.
- [57] Montesano J, Singh C. A synergistic damage mechanics based multiscale model for composite laminates subjected to multiaxial strains. *Mech Mater* 2015;83:72–89. <https://doi.org/10.1016/j.mechmat.2015.01.005>.
- [58] Montesano J, Chu H, Singh CV. Development of a physics-based multi-scale progressive damage model for assessing the durability of wind turbine blades. *Compos Struct* 2016;141(Febuary):50–62. <https://doi.org/10.1016/j.compstruct.2016.01.011>.
- [59] Zuo Y, Montesano J, Singh CV. Assessing progressive failure in long wind turbine blades under quasi-static and cyclic loads. *Renew Energy* 2018;119:754–66. <https://doi.org/10.1016/j.renene.2017.10.103>.
- [60] Nguyen TH, Gamby D. Effects of nonlinear viscoelastic behaviour and loading rate on transverse cracking in CFRP laminates. *Compos Sci Technol* 2007;67(3–4):438–52. <https://doi.org/10.1016/j.compscitech.2006.08.027>.
- [61] Berton T, Montesano J, Singh CV. Development of a synergistic damage mechanics model to predict evolution of ply cracking and stiffness changes in multidirectional composite laminates under creep. *Int J Damage Mech* 2015;0(0):1–19. <https://doi.org/10.1177/1056789515605569> <http://ijd.sagepub.com/cgi/doi/10.1177/1056789515605569>.
- [62] Berton T, Haldar S, Montesano J, Singh CV. Time-dependent damage analysis for viscoelastic-viscoplastic structural laminates under biaxial loading. *Compos Struct* 2018;203(May):60–70. <https://doi.org/10.1016/j.compstruct.2018.06.117> <https://doi.org/10.1016/j.compstruct.2018.06.117> <https://linkinghub.elsevier.com/retrieve/pii/S0263822318308286>.
- [63] Sánchez-Heres LF, Ringsberg JW, Johnson E. Effects of matrix cracking on the estimation of operational limits of Frp laminates. 15th eur. Conf. Compos. Mater. 2012. p. 1–8. June. ISBN 9788888785332.
- [64] Kobayashi S, Takeda N. Experimental characterization of microscopic damage behavior in carbon/bismaleimide composite - effects of temperature and laminate configuration. *Compos Part A Appl Sci Manuf* 2002;33(11):1529–38. [https://doi.org/10.1016/S1359-835X\(02\)00174-4](https://doi.org/10.1016/S1359-835X(02)00174-4).
- [65] Nairn JA, Hu S. The initiation and growth of delaminations induced by matrix microcracks in laminated composites. *Int J Fract* 1992;57(1):1–24. <https://doi.org/10.1007/BF00013005>.
- [66] Wu W, Owino J, Al-Ostaz A, Cai L. Applying periodic boundary conditions in finite element analysis. SIMULIA community conf. Providence. 2014. p. 707–19.
- [67] Schoeppner GA, Abrate S. Delamination threshold loads for low velocity impact on composite laminates. *Compos Part A Appl Sci Manuf* 2000;31(9):903–15. [https://doi.org/10.1016/S1359-835X\(00\)00061-0](https://doi.org/10.1016/S1359-835X(00)00061-0).
- [68] Menna C, Asprone D, Caprino G, Lopresto V, Prota A. Numerical simulation of impact tests on GFRP composite laminates. *Int J Impact Eng* 2011;38(8–9):677–85. <https://doi.org/10.1016/j.ijimpeng.2011.03.003> <https://doi.org/10.1016/j.ijimpeng.2011.03.003>.